metals

MDPI

Article

Degassing of Aluminum Alloy Melts by High Shear Melt Conditioning Technology: An Overview

Jaime Lazaro-Nebreda [1,*], Jayesh B. Patel [1], Ewan Lordan [1], Yijie Zhang [1], Erdem Karakulak [1], Kawther Al-Helal [1], Geoff M. Scamans [1,2] and Zhongyun Fan [1]

[1] Brunel Centre for Advanced Solidification Technology, Brunel University London, Uxbridge UB8 3PH, UK
[2] Innoval Technology Limited, Beaumont Cl, Banbury OX16 1TQ, UK
* Correspondence: jaime.lazaronebreda@brunel.ac.uk

Abstract: The search for more efficient methods for degassing aluminum alloy melts has always been of great interest for the metal industry because the presence of hydrogen and oxides in the melts' prior casting was detrimental to the integrity and properties of the final products. In this work, we present an overview of the progress and key findings from the research and development of an innovative High Shear Melt Conditioning (HSMC) degassing technology during the Liquid Metal Engineering (LiME) Research Hub project. Compared to conventional rotary degassing, this novel technique was capable of working at higher rotor speeds to efficiently break and disperse the naturally occurring oxide bifilms in the melt and to capture and disperse each supplied inert gas bubble into many tiny bubbles throughout the whole melt. This resulted in the elimination of the need to degas fluxes to remove the oxides in the melt, the reduction in the gas flow required to reach the same level of hydrogen removal rate, and the minimization of the regassing effect after processing. The increased process efficiency allowed for reduced melt processing costs and, at the same time, improved the melt quality, which resulted in fewer defects and improved mechanical properties.

Keywords: aluminum; high shear melt conditioning; degassing; oxide bifilm; hydrogen; recycling

Citation: Lazaro-Nebreda, J.; Patel, J.B.; Lordan, E.; Zhang, Y.; Karakulak, E.; Al-Helal, K.; Scamans, G.M.; Fan, Z. Degassing of Aluminum Alloy Melts by High Shear Melt Conditioning Technology: An Overview. *Metals* **2022**, *12*, 1772. https://doi.org/10.3390/met12101772

Academic Editor: Wislei Riuper Osório

Received: 31 July 2022
Accepted: 18 October 2022
Published: 21 October 2022

1. Introduction

Degassing is the most critical step for the aluminum casting industry, because it aims to ensure sufficient melt quality prior to solidification, producing high-quality cast products free of defects. The presence of dissolved hydrogen and solid oxide bifilms or inclusions causes porosity and cracks in the solidified components, and this is detrimental to the mechanical properties of the castings, so there is always a need to remove them from the melt prior to casting [1].

There are several degassing methods that are used by industry or that are under research and development. These mainly require generating multiple gas bubbles that are well-dispersed in the melt, which can capture the dissolved hydrogen by diffusion through the bubble–melt interface. This can be accomplished via the injection of inert or reactive purge gases through lances, although the process efficiency is low this way. The addition of fluxes or chemical dropping pellets, where the added solid material decomposes, liberating the gas bubbles in the melt (like an effervescent tablet in water), which increases effectiveness but requires either multiple steps or the use of a rotary impeller to improve the flux distribution. Other typical methods are vacuum degassing [2], ultrasonic degassing [3], spray degassing [4], filtration, and rotary degassing [5]. Among them, rotary degassing is the most popular method used in industry to clean aluminum melts because of its simplicity and excellent performance. However, the current rotary degassing technique, based on the use of rotor impellers to distribute gas bubbles throughout

the whole melt, lacks efficiency because it requires high gas flow rates and long processing times to be fully effective [6]. The impeller rotation also causes strong turbulences and a vortex near the surface, which reduces processing window operability, accelerates regassing, and facilitates the entrapment of oxides from the surface. Due to this, rotary degassing requires the use of covering fluxes or multiple degassing steps to ensure an effective cleaning process [7,8].

To overcome these problems, the Brunel Centre for Advanced Solidification Technology (BCAST), at Brunel University London, developed an innovative technology, based on intensive melt shearing [9] and denoted as High Shear Melt Conditioning (HSMC), which efficiently disperses injected bubbles and existing oxide bifilms into the melt. Contrary to conventional rotary impellers, it does not disturb the melt surface and prevents deterioration of the melt quality after degassing, thus facilitating a more efficient cleaning of the aluminum alloy melt, better integrity of the castings, and improved mechanical properties.

In recent years, part of the research during the LiME Hub project was focused on the development of the HSMC technology, its applicability, and understanding the mechanisms toward a more efficient degassing technique for degassing aluminum melts. Despite most of the results having been already published during the project, they have been presented as individual studies on particular aspects of the technology or the degassing process. This paper presents a general overview of the HSMC degassing technology, the key findings, and a more detailed description and discussion of the previously published results and the progress made during the LiME project. For this, we first present a comprehensive explanation of the origin of the hydrogen and oxides in the aluminum melts and a description of the degassing fundamentals and requirements for effective melt cleanliness and melt quality assessment. Then, we compare the current rotary degassing technique with the innovative rotor–stator HSMC technology, highlighting the advantages of the new method. We continue showing how the evaluation of the parameters' effect on the process efficiency has been performed and discuss the importance of understanding the gas–liquid mixing diagrams to optimize the technique. After that, a summary of the results of the effect of HSMC degassing on melt quality, casting integrity, and mechanical properties is presented, and the processing–structure–properties relationship and the importance of a good melt quality assessment are discussed. Finally, we present the current state of the technology's development and some of the latest scaling-up activities and discuss the potential technology implementation in industry.

2. Origin of Hydrogen and Oxides and the Assessment of Melt Quality

The major factors influencing the quality of aluminum alloy melts are dissolved hydrogen and the presence of oxide films, or more precisely oxide bifilms [10]. Both hydrogen and oxide bifilms are consequence of the reaction of the ambient moisture with the liquid aluminum surface, as described in Equation 1.

$$2Al + 3H_2O \rightarrow Al_2O_3 + 6H \quad (1)$$

The reaction produces atomic hydrogen, which is dissolved into the melt, and a thin oxide layer on the melt surface. When the melt surface is disturbed during handling, this layer breaks and folds over, entrapping air inside and becoming entrained inside the melt. The oxide bifilm, therefore, presents two sides, an outer wet side in contact with the liquid aluminum and an inner dry side in contact with the entrapped air.

Typically, hydrogen has been considered as the main originator of porosity in castings due to its different solubility in solid and liquid aluminum. During solidification, the hydrogen in excess would precipitate and recombine as molecular gas, causing the gas porosity. However, recent studies [11] have shown that hydrogen gas cannot nucleate in liquid aluminum either homogeneously or heterogeneously, but rather it precipitates in the already-existing gaps in the liquid or into the interdendritic regions at the final stages

of solidification. In that sense, Dispinar and Campbell described [12,13] that the oxide bifilms play a more important role in the formation of porosity by unfolding during solidification and letting the excess hydrogen diffuse into the gap within the bifilm sides, thus contributing to expand an already existing defect. The presence of this bifilm defect in the microstructures has a direct influence on the degradation and variability of the tensile and the fatigue mechanical properties of the castings [14–16].

Therefore, melt degassing techniques must focus on the removal of not only hydrogen but also, more importantly, the entrapped oxide bifilms from the melt, to ensure sufficient melt quality and to reduce the potency of porosity formation during solidification.

The quality of the aluminum melts before and after the degassing process can be evaluated by different techniques [17]. The hydrogen content in the melt can be directly measured using a FOSECO ALPEK-H probe (EMC Hycal, Limited, Stafford, UK) [18] immersed in the melt, with the measurement given as mL/100 g Al. However, this technique only gives information about the hydrogen level, not about the content of the oxides in the melt. Another technique to account for both hydrogen and oxide bifilm content is the reduced pressure test (RPT) [12,13], which involves solidifying the melt into two conical steel cups, one in air (atmospheric pressure) and the other under partial vacuum pressure (80 mbar). The melt quality is then evaluated by calculating the Density Index (DI%) using Equation 2, where D_{air} and D_{vac} are the density of the samples solidified in air and under vacuum, respectively. The more hydrogen and oxides in the melt, the higher the Density Index is.

$$DI\ (\%) = 100 \times (D_{air} - D_{vac}) / D_{air} \quad (2)$$

The RPT samples can be also cut and polished to evaluate the aspect of internal porosity developed during the solidification, which is an indirect indicator of the potential porosity to be generated in the castings. In that sense, another method more recently used to quantify the melt quality based on the RPT sampling is the so-called Bifilm Index (BI) assessment. The Bifilm Index is defined, by Equation 3, as the sum of the length of all pores identified in the surface of the RPT cross section [19]. Despite being more complex or time-consuming to evaluate, i.e., requiring cutting and assessing the RPT sample surface, the Bifilm Index is considered a better indicator of the melt quality [20], as it accounts only for the oxide content in the melt, while the Density Index accounts for the combined effect of both oxides and hydrogen content in the melt, and this might hinder or scatter the real impact of the oxides in the generation of cracks and porosity in the solidified castings. However, due to its simplicity and faster calculation, the Density Index assessment is still the main technique used in industry for evaluating the quality of aluminum melts.

$$BI = \sum pore\ lenght \quad (3)$$

3. High Shear Melt Conditioning Development for Degassing

3.1. Requirements for Achieving an Efficient Degassing

A degassing technique is considered efficient if it can provide a fast cleaning at a low cost, both in terms of energy and material consumption. At the same time, it needs to keep surface turbulences to a minimum, be able to eliminate most of the hydrogen and oxide bifilms in the melt below certain limits, and guarantee sufficient melt quality for a long time after processing to avoid the need for repeated degassing cycles.

The conventional rotary degassing approach injects inert gas bubbles and distributes them in the whole volume with the help of a rotor impeller. During the degassing process, the level of hydrogen that remains dissolved in the melt as a function of time can be described by Equation 4 [6], where H_{eq} denotes the equilibrium solubility level of the hydrogen in the aluminum melt, H_0 denotes the initial hydrogen content, K_b denotes the diffusion coefficient of hydrogen at the melt/bubble interface, A_b denotes the total interfacial area of the bubbles, and V_m denotes the total volume of melt being processed.

$$H(t) = H_{eq} + (H_0 - H_{eq}) \exp(-K_b A_b t/V_m) \quad (4)$$

At the same time, the buoyancy of the bubbles toward the surface is another important parameter to control, because it determines the residence time of the bubbles in the liquid capturing the dissolved gases. The flotation speed of the bubbles can be expressed by Equation 5 (Stokes law), where V is the bubble velocity, ϕ is the diameter, g is the gravity acceleration, η is the fluid viscosity, and ρ is the densities of the gas and liquid phases.

$$V = \phi^2 g (\rho_{gas} - \rho_{liquid})/(18\eta) \quad (5)$$

One could consider that increasing the gas flow is beneficial because it offers a larger bubble surface area to capture the dissolved hydrogen efficiently [21], but this also causes a faster flotation of the bubbles toward the surface, thus reducing their residence time in the melt and making the process less efficient above a certain gas flow [22]. Therefore, increasing the rotor speed to reduce the bubble size is always the best approach [5,6]. However, increasing the rotor speed in conventional designs causes a vortex and surface turbulences, which facilitate the reabsorption of hydrogen and the entrapment of new oxide films in the melt (regassing), as it is shown in Figure 1a. Therefore, the rotor speed cannot be too high in conventional rotary degassing. Baffles are used in industry to minimize the vortex, but they are only effective to a certain extent.

On the other hand, bubble mixing does not totally solve the problem of the oxide bifilm's presence in the aluminum melts, because it is able to remove the larger oxides but not the smaller ones [23,24], and, therefore, the use of fluxes is always a must when using rotary degassers [8], which ends up increasing the process costs and generating more dross (losses).

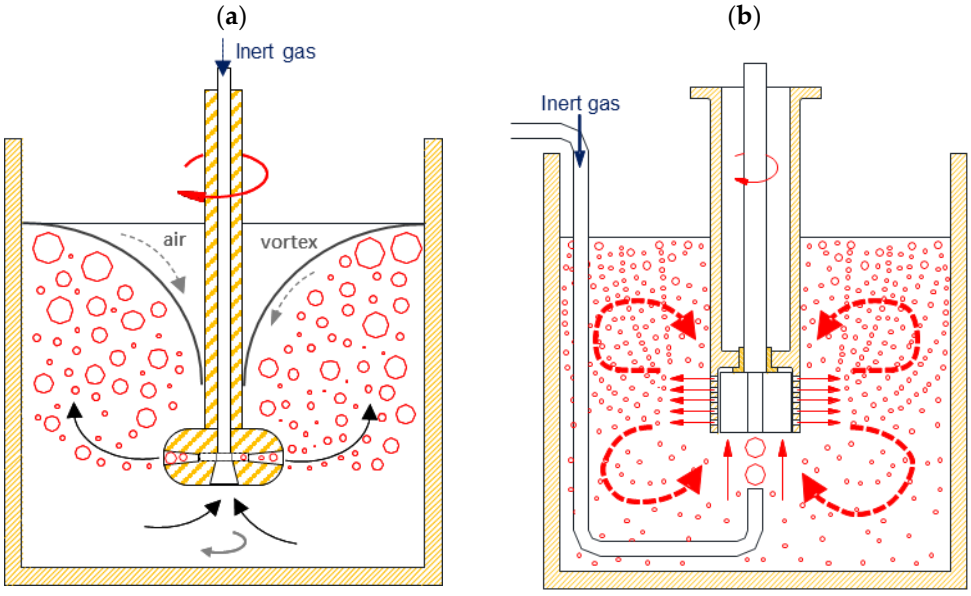

Figure 1. Schematic diagrams of (**a**) conventional rotary degassing and (**b**) HSMC degassing methods. The arrows indicate the flow pattern of the bubbles in the melt. Adapted from [24].

3.2. From the Conventional Rotary Methodology to the Innovative HSMC Degassing Process

Regarding the problems mentioned above for the rotary degassing methodology, BCAST found, a few years ago [25], that oxide bifilms can be efficiently dispersed into fine particles using an advanced twin-screw high shear technology. When combined with inert gas [26], it could also significantly reduce the hydrogen content in the melts. From there, a new configuration was developed at BCAST [9].

A schematic diagram of the technology, denoted as High Shear Melt Conditioning (HSMC), is shown in Figure 1b. It is comprised of a rotor–stator arrangement made from an inert ceramic material, which extends its lifetime compared to current graphite impellers. The gas is not injected through the rotor shaft, but by an external pipe located underneath the high shear unit, a configuration that facilitates the capture of the bubbles [27]. A more detailed description of the technology, its operation, and the experimental conditions for the results shown later in this paper can be found in a recent publication [24].

During its operation, the rotation speed can vary, in the range of 1000–10,000 rpm, providing an extremely high shear rate (up to $10^5\ s^{-1}$). This high shear rate is the result of the melt being pumped upwards from the bottom and then squeezed in between the small rotor–stator gap and through the openings of the stator. The liquid is projected radially, as high-velocity jets, toward the wall of the crucible, where it splits into upper and lower flow patterns (dashed arrows in Figure 1), while more liquid is being pumped into the unit. The stator acts as a built-in baffle and prevents the high rotor speeds from generating a centrifugal flow and the origination of a surface vortex. The technology provides not only a macroflow in a large volume of melt for distributive mixing, as typically rotary degassers only do, but also provides a microflow with an intensive shearing effect near the tip of the device, for dispersive mixing. A more detailed description of the technology and its operation can be found in a recent publication [24]. During the LiME Hub program, two units (42 and 90 mm in diameter) were manufactured and tested. In the first part of this paper, we focus mainly on the results from the 42 mm unit, as the key findings and conclusions are independent of the unit size, though we show some of the latest results for the 90 mm unit at the end.

3.3. HSMC Process Visualization and Optimization by Water Modeling

Physical modeling of the technology process in water was conducted to visualize the effect of high shear degassing parameters (rotor speed and gas flow) on the dispersion and distribution of the inert gas bubbles in the liquid [24,28]. Water shares a similar fluid dynamic behavior (viscosity to density ratio) with molten aluminum, and, therefore, it is an excellent liquid to replicate bubble dispersion and degassing performance in molten aluminum [29,30]. Examples of these visualizations are shown in Figure 2, for the HSMC 90 mm unit compared to the FOSECO 90 mm rotary degasser available in our laboratory (Foseco, Tamworth, UK), and in Figure 3, for the HSMC 42 mm unit evaluation and process optimization. The water tank dimensions and unit positioning were selected as close as possible to the experimental plan with molten aluminum. This allowed for the direct implementation of the observations in water into the aluminum melt processing, with minimal adjustments.

3.3.1. Improved Bubble Dispersion and Surface Stability Compared to Rotary Degassing

Figure 2 shows a visual comparison of the HSMC degassing unit (Figure 2a) with the current rotary degasser available in our laboratory (Figure 2b); both are 90 mm in diameter, when applied in a water tank. What can be noticed first is that the rotor–stator unit can be operated at a higher rotor speed without the generation of a vortex or strong surface turbulences, which normally occur during rotary degassing and require the use of baffles to minimize their effect and slow down the entrapment of new oxides and air into the melt. This allows for increasing the process efficiency, by significantly reducing the amount of inert gas flow required to reach an effective bubble-dispersion regime in whole volume. This happens because, with HSMC, all the bubbles are captured and finely dispersed and distributed, while in rotary degassing some bubbles can escape directly to the surface without been dispersed. Furthermore, the strong macroflow provided by the HSMC technology allows for reducing the unit-immersion depth in the liquid required for an effective bubble dispersion; rotary degassing mostly distributes the bubbles above the mixing head, so it normally needs to be immersed close to the bottom of the furnace to be more effective.

On the other hand, the bubbles dispersed with the HSMC technology are much smaller, and their size can be controlled by the rotor speed [31,32]. The overall interfacial area between the bubbles and the liquid increases significantly [24], which, combined with their uniform dispersion, contributes to a larger diffusion of the dissolved gasses from the liquid into the bubbles. The buoyancy of the bubbles toward the surface is drastically reduced, and, therefore, tiny bubbles can remain for a longer time in the liquid, capturing the dissolved gases, as already mentioned when introducing Equation 2.

In addition to this, HSMC can also break and homogeneously disperse the inclusions present in the liquid, while a rotary degassing system can only distribute them, as shown by the dark particles marked with arrows in Figure 2b, which are not visible in Figure 2a.

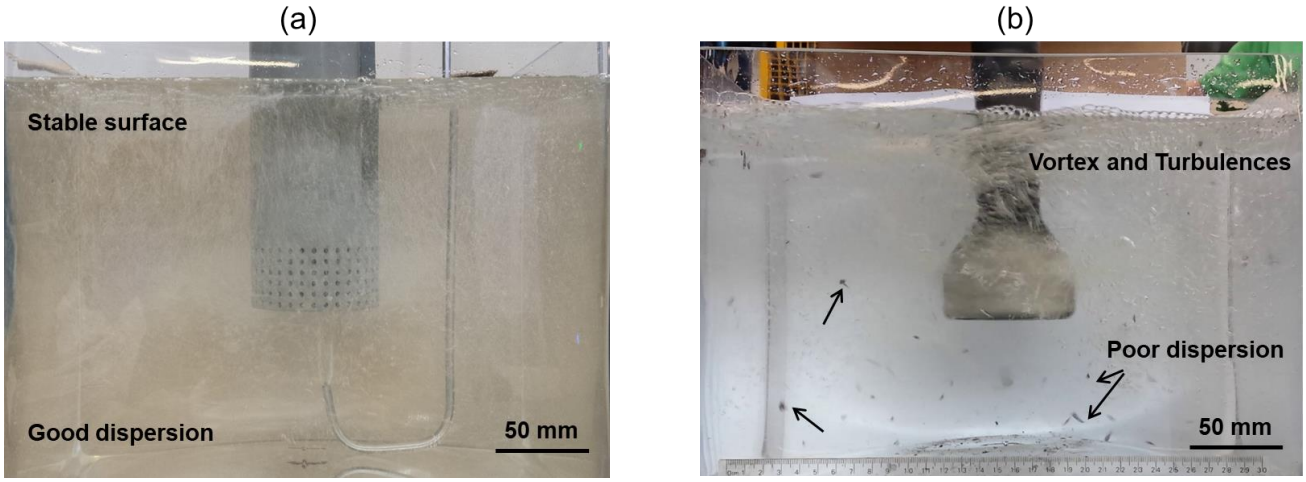

Figure 2. Visualization in water of (**a**) HSMC degassing (1000 rpm, 0.5 L/min), offering distributive and dispersive mixing and stable fluid surface. (**b**) Rotary degassing (350 rpm, 5 L/min) offers only distributive mixing, poor dispersion, and vortex surface turbulence. The black arrows indicate the presence of non-dispersed particles in the liquid.

3.3.2. Effect of Rotor Speed and Gas Flow Rate on the Dispersion of Bubbles by HSMC

Figure 3 shows the effect of varying the rotor speed and gas flow rate on the dispersion of bubbles in water, using the 42 mm HSMC degassing unit [24]. The bubble flow and volume of liquid covered by the dispersed bubbles have been highlighted with dashed arrows. They increase with rotor speed and decrease with the gas flow rate. Three main regimes associated with the gas–liquid mixing can be defined in mechanically agitated systems [33]: Flooded, Loaded, and Dispersion. A fourth regime, denoted as Recirculation, can be also considered as an evolution or extension of the dispersion regime [34–37].

For low rotor speeds, the system is in the Flooded regime (Figure 3a,e), in which the gas bubbles are hardly dispersed or distributed, covering just the volume near the degasser and quickly escaping directly to the surface. As the rotor speed increases, the mixing moves to the Loaded regime (Figure 3b,f), where bubbles are dispersed, so they are only observed in the volume above the mixer. Above certain rotor speeds, the bubbles start also being observed below the mixer (Figure 3c,g), transitioning the system to the Dispersion regime. Finally, the system reaches the Recirculation regime, when the dispersed bubbles reach a size small enough to be dragged again into the mixer and re-dispersed (Figure 3d,h). Under this regime, a significant fraction of the injected gas never has a chance to escape the macroscopic flow, only doing so when the mixer is stopped and the liquid is left to rest.

Therefore, increasing the gas flow rate requires a higher rotor speed to achieve bubble recirculation. Both high gas flow and high rotor speed can cause surface instabilities (Figure 3e–h). On the other hand, for a low gas flow rate, the minimum rotor speed required for recirculation decreases, and the surface remains more stable (Figure 3a–d).

The power consumption for the rotor–stator unit can be described by Equation 6 [38], where D is the rotor diameter, N is the rotor speed, ρ is the fluid density, and N_P is the power number, which depends on mixer geometry but is constant with respect to the rotor speed and diameter under turbulent conditions, i.e., $Re > 10^4$, as in the case of HSMC flow [39]. From this, we can see that reducing the gas flow also allows for a significant reduction in the process' power consumption.

$$P = N_P \rho N^3 D^5 \quad (6)$$

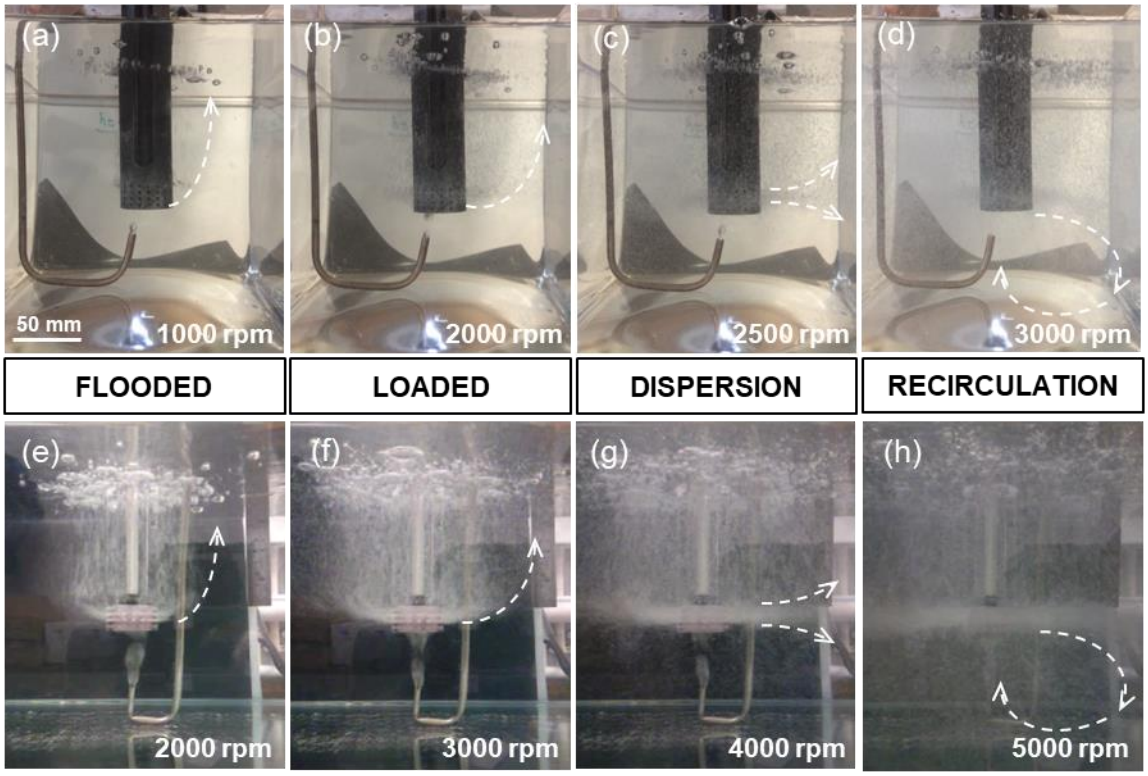

Figure 3. Visualization in water of the effect of gas flow rate and rotor speed on the bubble dispersion during HSMC degassing processing: (**a**–**d**) 0.1 L/min; (**e**–**h**) 1.0 L/min. The arrows indicate the flow pattern of the bubbles in the melt. Adapted from [24].

Therefore, the optimum operational window requires a low gas flow rate (< 1 L/min) and a rotor speed between 3000 rpm and 6000 rpm. This can be better observed in Figure 4, which represents the gas–liquid mixing regimes map, associated with the configuration shown in Figure 3. The map has been created using the data and analysis presented in previous studies [24,31,40]. The prediction of the regime transitions is key from an industrial point of view, especially from flooded to loaded [41], as it defines the minimum operating conditions, but the loaded to dispersed or full recirculation transition is more important, as it allows for the maximization of the process efficiency [37].

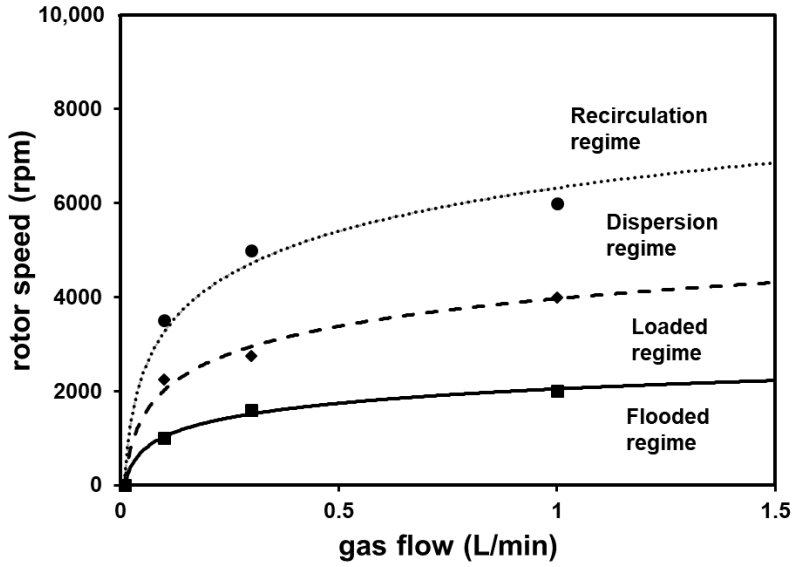

Figure 4. Effect of gas flow rate and rotor speed on the bubble dispersion during HSMC in water. Diagram predicted using the data published in previous studies [24,31,40].

The gas–liquid mixing regimes map can be made scale independent [36], if gas flow (q) and rotor speed (N) are substituted by the dimensionless parameters H (geometry number; D/T), Q (Flow number; $qN^{-1}D^{-3}$), and Fr (Froude number; N^2Dg^{-1}), where D and T are the impeller and tank diameter. The boundaries between the flow regimes can be obtained using Equation 7 for the loaded regime, Equation 8 for the dispersion regime, and Equation 9 for the full recirculation regime [34,37]. For the case of the HSMC 90 mm diameter unit, when considering a gas flow of 0.5 L/min, the regime transitions are satisfied at around 350 rpm for flooded to loaded, at 650 rpm for loaded to dispersed, and at 1100 rpm for dispersion to recirculation (see Figure 2a), which are the conditions already used and validated in previous studies [42,43].

$$Q < 30FrH^{3.5} \quad (7)$$

$$Q < 0.2Fr^{0.5}H^{0.5} \quad (8)$$

$$Q < 13Fr^{2}H^{5} \quad (9)$$

4. Applicability of HSMC on Aluminum Melts

4.1. Materials, Degassing, and Casting Procedure

The main studies during the technology's development and testing have been conducted on the secondary aluminum alloy, with an approximate composition of Al-(6.8–7.5)Si-(0.3–0.5)Mg-(0.12–0.25)Fe, i.e., an A356/LM25-type alloy [24,32]. However, the technology has also been successfully tested on other aluminum alloys such as the A380/LM24 [42] and Silafont-36 (AlSi10MnMg) [43] HPDC alloys, the Zorba cast fraction scrap (~LM27) [44], the 7032 [31,45], 7075 [9,40], and 2024 [46] wrought alloys, and also for recycling the A20X alloy (Aeromet [47]) prepared from recovered scrap material. In all these cases, a significant reduction in hydrogen and in oxide bifilm content were found, when compared to conventional rotary degassing.

For the degassing studies, the material was melted, in charges ranging from 6–10 kg for the laboratory scale trials and up to 50–500 kg for the large-scale trials, in clay graphite crucibles using electrical resistance furnaces at temperatures from 700 °C to 750 °C and held for at least one hour for homogenization. Each time the unit was then immersed

halfway from the melt surface to the bottom of the crucible and operated at the minimum rotor speed, obtained from water modeling, for each inert gas flow rate, to ensure full bubble dispersion in the melt.

After degassing, the melts were skimmed and isothermally held in the furnace to rest. No granular flux was used during degassing or to cover and protect the surface of the melt afterwards, to allow for natural regassing to occur during the holding period. The melt quality was assessed at different times, during both the degassing and holding stages, by RPT sampling and by assessing the structural integrity and the mechanical properties of the tensile bars cast into the ASTM B108 standard permanent steel mold [48] and tested in accordance with ASTM E8-03 [49]. Details of the degassing, casting, and testing conditions for the tensile speciments can be found in a previous paper [24].

4.2. Faster and More Efficient Removal of Hydrogen and Oxide Bifilms from the Aluminum Melts

Figure 5 and Table 1 show the comparison of a standard rotary degassing procedure with HSMC degassing and the effect of the processing parameters on the Density Index and the hydrogen content in the melt. The three melts started with similar conditions (DI ~ 10%–15%; H ~ 0.36 mL/100 gAl), and the degassing process was monitored with an Al-spek-H probe and stopped when the hydrogen content was decreased below 0.1 mL/100 gAl.

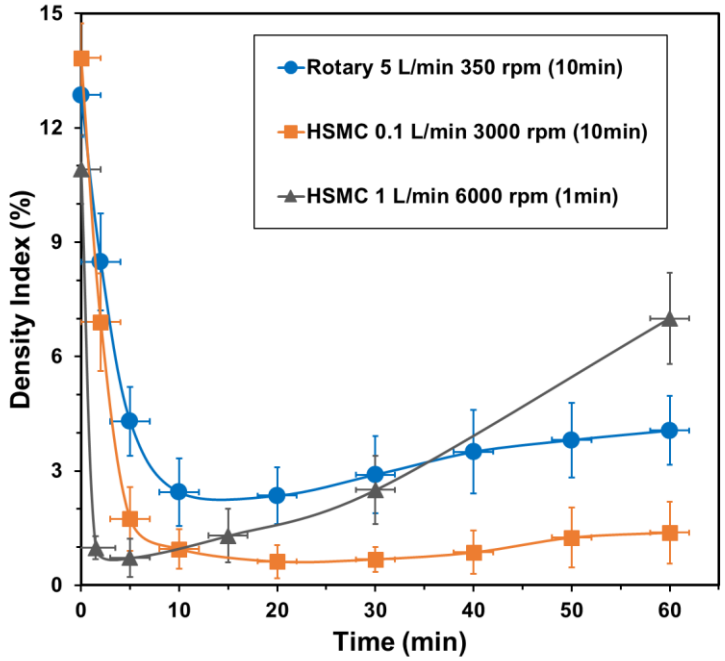

Figure 5. Comparison by Density Index evaluation of the HSMC degassing performance with conventional rotary degassing. Data points replotted from results in previous studies [24,32].

After degassing, both rotary and HSMC are very effective at degassing, reaching Density Index values below the accepted industrial limit, i.e., DI < 3% [50]. However, the values after HSMC degassing are considerably lower, with DI < 1%. Despite using a much lower gas flow rate, degassing is achieved in a shorter time due to the already mentioned larger bubble surface area and effective bubble dispersion. The results also highlight the effective elimination of the hydrogen present in the melt. While the HSMC at the 0.1 L/min and 3000 rpm operating condition requires between 5 and 10 min, similar to rotary degassing, the HSMC at the 1 L/min and 6000 rpm operating condition only requires 1 min to reach similar results. This is because the higher rotor speed used is expected to disperse

the bifilms and the bubbles much faster within the melt, and the higher gas flow is expected to increase the overall surface area for hydrogen diffusion.

Table 1. Hydrogen content (X ± 0.02 mL/100gAl) in the melt before and after degassing for 10 min.

Trial	Before	After Degassing	After Holding 60 Min
Rotary 5 L/min–350 rpm [1]	0.38	0.08	0.10
HSMC 0.1 L/min–3000 rpm [1]	0.37	0.06	0.09
HSMC 1 L/min–6000 rpm [2]	0.35	0.06	0.11

[1] Degassing for 10 min [24]; [2] degassing for only 1 min [32].

However, after degassing, all melts naturally tend to reabsorb hydrogen due to the reaction of the melt surface with the ambient humidity, and it is only then when the real effect on oxide bifilm elimination can be really appreciated. In that sense, both the rotary and HSMC at 1 L/min–6000 rpm degassed melt should be used within the first 30 min, otherwise the Density Index becomes higher than 3%. On the other hand, the HSMC at the 0.1 L/min–3000 rpm degassed melt does not exhibit an increase in Density Index; even after one hour, the hydrogen in the melt reaches almost a similar level as the other melts.

The significant regassing observed for the HSMC at the 1 L/min–6000 rpm process can be explained in terms of: (i) the short processing time (~1 min), which might have been effective for bubble dispersion but not enough for bifilm refinement; (ii) the fact that a larger gas flow in the rotor–stator gap reduces the efficiency for oxide dispersion; (iii) a higher gas flow and rotor speed cause more surface turbulences (Figure 3e–h) that can entrap oxides and air back into the melt, which quickly turn into porosity, and the Density Index increases as soon as hydrogen diffuses back in the melt.

On the other hand, for the HSMC at the 0.1 L/min–3000 rpm process, the regassing is minimized because: (i) it has had more time to act on the bifilms; (ii) the gas fraction in the rotor–stator is much lower, making the dispersion of oxides more effective; (iii) the melt surface remains more stable (Figure 3a–d); (iv) the dispersed bubbles remain longer in the melt until they reach the surface, acting as a protective layer against hydrogen reabsorption [24,32]. Therefore, the HSMC at the 1 L/min–6000 rpm melt would probably need to be degassed for longer to ensure bubbles and oxide-bifilm dispersion. This makes the HSMC at the 0.1 L/min–3000 rpm melt more efficient in terms of volume of gas [51] and unit power consumption [38] and ensures the melt quality for longer after processing, which is crucial in industry to avoid the need for repeated degassing cycles before casting [3].

5. Effect of HSMC Degassing on Casting Integrity and Mechanical Properties

5.1. Significant Reduction in Porosity Size and Defects in the Castings

Figure 6 shows the vertical cross sections of the RPT samples solidified under a partial vacuum, before and right after degassing with the rotary and HSMC methods. Before degassing, the RPT sample exhibits a significant pore density of 37 cm^{-2} of large round pores (~650 μm in diameter), with a convex top surface due to the porosity generation, and subsequent expansion during the solidification under vacuum. After degassing, the top surface of the RPT samples acquires a concave shape in all cases, due to the lower porosity formed during the solidification, and the internal porosity is reduced in terms of size and number density. However, despite the similar hydrogen content, the degassed RPT samples show a different level of porosity, which clearly highlights the dissimilar presence of oxide bifilms in the melt [10]. The rotary sample shows an average pore size of 340 μm and pore density of 22 cm^{-2}, which is reduced to 105 μm in diameter and 11 cm^{-2} pore density for the HSMC at 0.1 L/min–3000 rpm and to ~150 μm pore size and 15 cm^{-2} pore density for the HSMC at 1 L/min–6000 rpm. This again suggests that the HSMC at 1 L/min–6000 rpm for 1 min is not as effective for degassing as the HSMC at 0.1 L/min–

3000 rpm for 10 min, so either the first would need more time, in detriment to the process efficiency, or the gas flow reduced, to reduce costs and increase consumption efficiency.

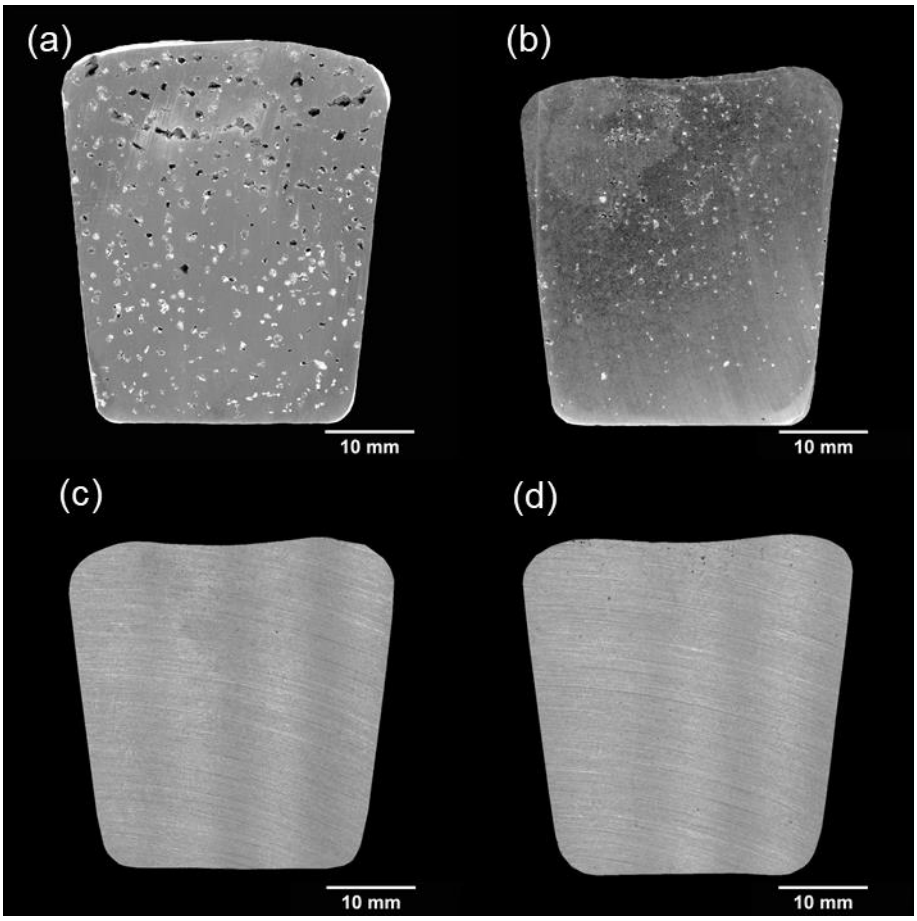

Figure 6. Porosity of the vacuum RPT samples obtained (**a**) before degassing; (**b**) after rotary degassing; (**c**) after HSMC 0.1 L/min–3000 rpm degassing; (**d**) after HSMC 1 L/min–6000 rpm degassing. Adapted from [24,32]. Reprinted with permission from [32]. Copyright 2022 Elsevier.

The effect of holding time after degassing on the internal aspect of the RPT samples solidified under partial vacuum is shown in Figure 7. By increasing the holding time and hydrogen reabsorption through the melt surface (Table 2), the remaining oxide bifilms in the melt after degassing have more chances to unfold and be filled with the excess hydrogen, thus resulting in a significant porosity and Density Index increment. When the melt quality becomes deteriorated with time (Figure 7a,c), the pore formation in the castings increases linearly [23,52], and, consequently, the mechanical properties decrease significantly. When this happens, the only solution is to repeat the degassing process. Therefore, to ensure that the melt maintains a low Density Index and low RPT porosity size for a long time after degassing (Figure 7b), regardless of the hydrogen content in the melt, it is necessary to guarantee the elimination of the oxide bifilms.

Table 2. Analysis of the porosity in RPT samples collected and solidified under partial vacuum during the in-line HSMC degassing process at a melt flow rate of 2 kg/min. Analysis of samples from [28].

Rotor Speed (rpm)	Average Pore Diameter (μm)	Pore Density (pores/cm^{-2})	Bifilm Index (mm)
0	750 ± 150	20 ± 4	210 ± 20
500	500 ± 80	17 ± 5	114 ± 22
1000	400 ± 60	15 ± 5	74 ± 13

1500	300 ± 40	12 ± 5	68 ± 11
2000	250 ± 30	8 ± 3	24 ± 7

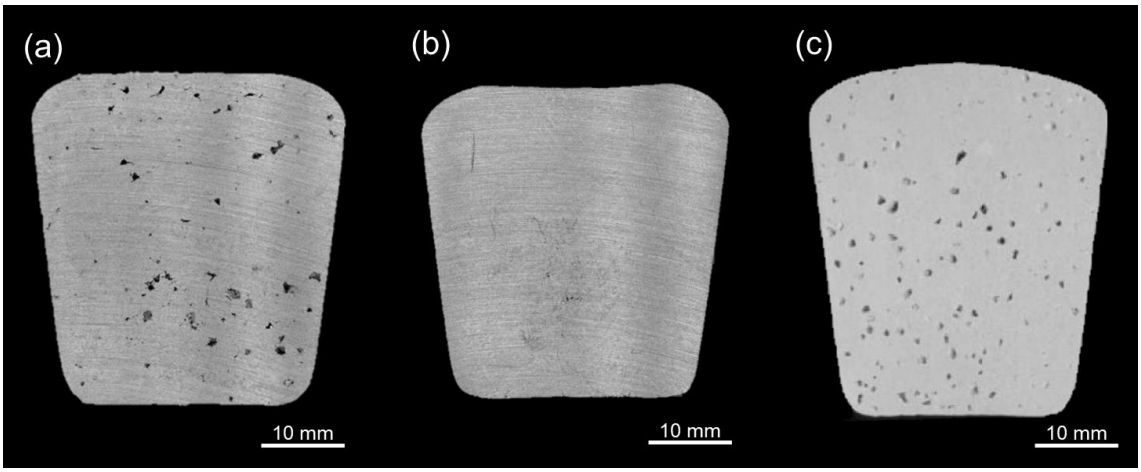

Figure 7. Porosity of the vacuum RPT samples obtained after holding the melt for 1 h after degassing. (**a**) Rotary; (**b**) HSMC 0.1 L/min–3000 rpm; (**c**) HSMC 1 L/min–6000 rpm. [24,32]. Reprinted with permission from [32]. Copyright 2022 Elsevier.

It is recognized that the resulting microstructural arrays are affected by the applied operational parameters. The cooling rate is an important mechanism to refine the microstructure. Besides, the mechanism including degassing melting has also refined the resulting microstructural array [26,44]; consequently, it has an important role upon the distinctive material's properties [53–55].

Figure 8 shows an example of the typical fracture surfaces of postmortem tensile bars and how they change depending on the effectiveness of the degassing method used. The experimental conditions for obtaining such samples re provided in a previous study [24]. Two types of defects can be identified on the fracture surface: gas porosity and oxide films. The fracture surface of the sample cast after rotary degassing (Figure 8a) exhibits roughness, gas porosity, and large and small oxide films. On the contrary, the fracture surface of the tensile bar cast after HSMC degassing (Figure 8b) presents a smoother surface with fewer and smaller oxide-type defects, and no gas porosity is observed.

The presence of these defects affects the mechanical properties because it reduces the effective cross section, and, when the stress is applied, it is concentrated in a smaller region, thus causing the sample fail earlier [56]. This also affects the mechanical properties' variability. Samples solidified under similar conditions can exhibit different properties just because of a small variation in the content of the inclusions in the cross section of the bar. Therefore, it is important to properly quantify the area fraction of the defects in the fracture surface. This is typically accomplished postmortem by optical image analysis [57] but can even be completed before mechanical testing by means of X-ray tomography and advanced 3D image analysis [58]. The idea, in this case, is to anticipate, by measuring the cracks in the sample and the effective areal fraction of the defects perpendicular to the tensile direction, and use the results to predict the detrimental effect on the mechanical properties.

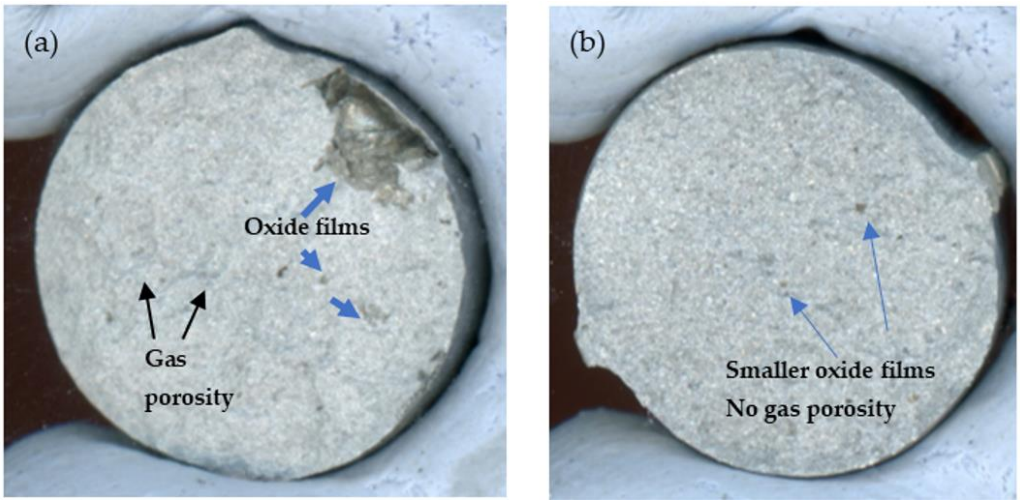

Figure 8. Fracture surfaces of postmortem tensile bars that were cast after (**a**) conventional rotary degassing and (**b**) HSMC degassing. Representative samples are from a previous study [24].

The measured area fraction of the defects found in the fracture surface of the postmortem tensile bars can be also correlated by the evaluation of the melt quality before casting. Figure 9 plots the comparison of the area fraction of the defects versus the hydrogen level in the melt (Figure 9a) and the corresponding comparison versus the calculated Density Index (Figure 9b), for tensile bars cast before and after degassing with the rotary or HSMC techniques. Both graphs have been created by combining the data presented in a previous study [24]. A linear correlation is observed in both cases, but the variation of the defect content with hydrogen content in the melt is more scattered and exhibits a lower coefficient of determination (R^2 = 0.8056). On the other hand, the linear correlation between the fraction of defects and the Density Index is less scattered and presents a higher coefficient of determination (R^2 = 0.9695). This implies, as expected, that the Density Index is a better indicator of the melt quality and that it can be used to estimate, with good accuracy, the potency of the melt to produce castings with different levels of defects, because it accounts for both the oxide bifilms and the hydrogen in the melt, i.e., the two originators of porosity.

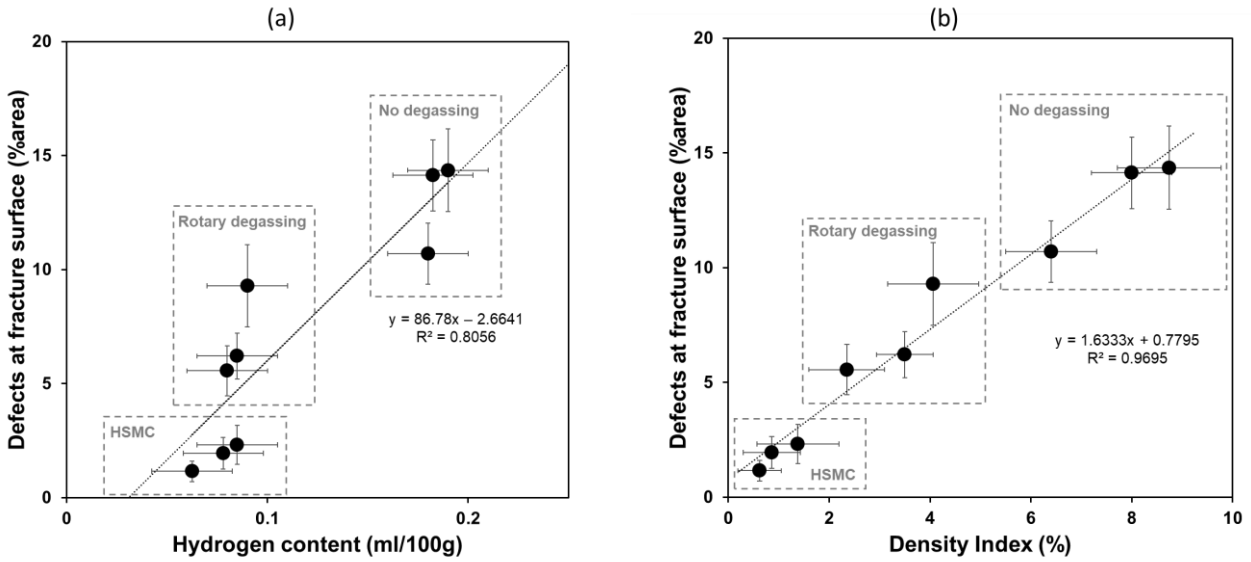

Figure 9. Area fraction of defects at the fracture surface of postmortem tensile bars versus the melt quality before and after degassing, evaluated by (**a**) hydrogen content and (**b**) Density Index. Adapted by combining data from results in a previous study [24].

5.2. Improved Mechanical Properties with Reduced Variability

Figure 10 presents a comparison of the mechanical properties of tensile bars before and after degassing an A356 alloy melt. A description of the evolution of these properties with time can be found in a recent study [24], while Figure 10 represents the average values and error ranges for the yield strength (YS), the ultimate tensile strength (UTS), and the elongation at break (El) from sets of samples collected before degassing and at different times up to 1 h after degassing. From Figure 10, it can be observed how HSMC produces higher values of UTS and elongation, while the yield strength remains unaffected by the degassing method. Furthermore, HSMC promotes a reduced variability in the properties, a result that has been confirmed in various studies for different alloys and casting conditions [42,43].

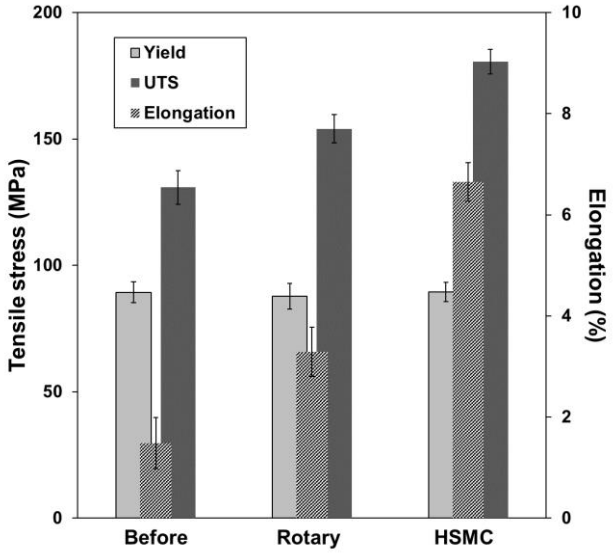

Figure 10. Mechanical properties of tensile bars cast before degassing and after processing by rotary degassing (5 L/min–350 rpm) and by HSMC degassing (0.1 L/min–3000 rpm). Average values from results in [24].

Given the fact that the fraction of defects in the castings correlates linearly with the melt quality (Figure 9) and the known correlation of this parameter with the mechanical properties [56–58], Figure 11 directly presents the correlation of the melt quality, by means of the Density Index, with the ultimate tensile strength and the elongation of the tensile bars before and after degassing an A356 alloy melt with the rotary and HSMC methods. In this case, the correlation fits very well to a logarithmic function type [58] for both the UTS and elongation dependences on the Density Index. Therefore, the Density Index is also a good indirect indicator of the variation of mechanical properties. Under appropriate calibrations, it could be even used as an estimator of the expected UTS and elongation before testing, without the need to use premortem CT [58] or postmortem optical [57] analysis on the fracture, which is especially practical as the shape of the castings becomes more complex.

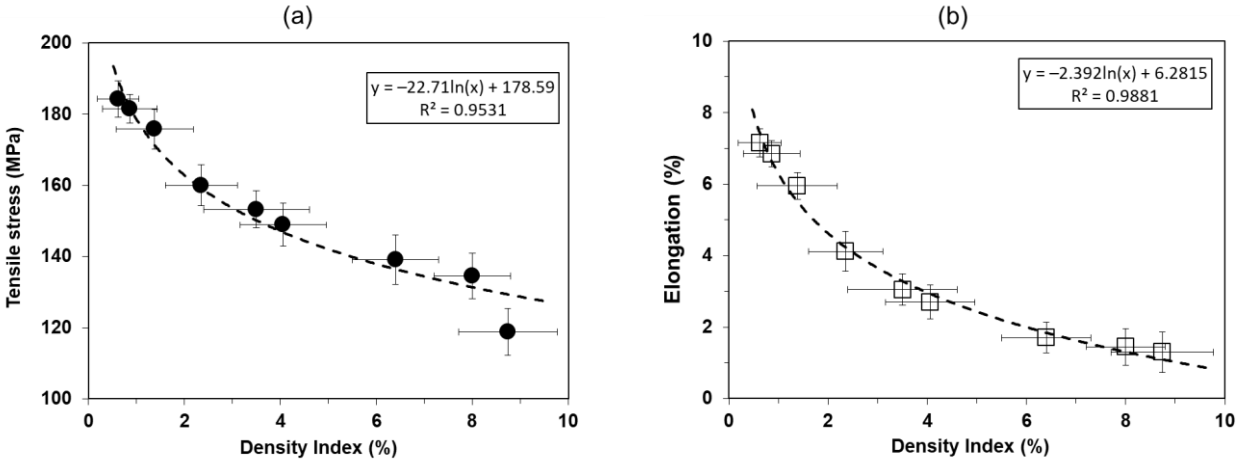

Figure 11. Correlation between the mechanical properties of the tensile bars and the Density Index values obtained by evaluating the melt quality before and after rotary and HSMC degassing. Adapted by combining data from results in a previous study [24].

6. Toward Implementation of the HSMC Degassing Process in Industry

In the previous sections, we have demonstrated how the HSMC technology performs at a laboratory scale and in relatively small batches. However, industry requires processing much larger amounts of melt and in relatively short times, thus requiring a larger melt flow processing rate. The net melt flow (Q) passing through the stator holes can be expressed by Equation 10 [38], where Nq is the flow number and depends on the unit geometry and rotor–stator configuration [39]. Therefore, the melt processing flow can be increased by increasing either the rotor speed or the unit size. However, this needs to be accomplished with precaution, as the power consumption also increases, more quickly, with the increment of these parameters (Equation 6).

$$Q = Nq\ ND^3 \tag{10}$$

In this section, we cover a summary of the key activities carried out, with the aim of scaling up the technology and increasing the technology readiness level (TRL). Firstly, we have explored the use of the larger 90 mm diameter unit on large-capacity crucibles. Secondly, we have explored the use of the small 42 mm diameter unit, while implemented in continuous mode.

6.1. Large Scale Batch Processing by HSMC Degassing

Figure 12 shows the different steps of the scale-up activities for implementing the HSMC 90 mm diameter unit on a large crucible with a capacity for 500 kg of aluminum melt, which is used for large-scale low-pressure die casting (LPDC) activities in the Advanced Metal Casting Centre (AMCC) building at Brunel University London.

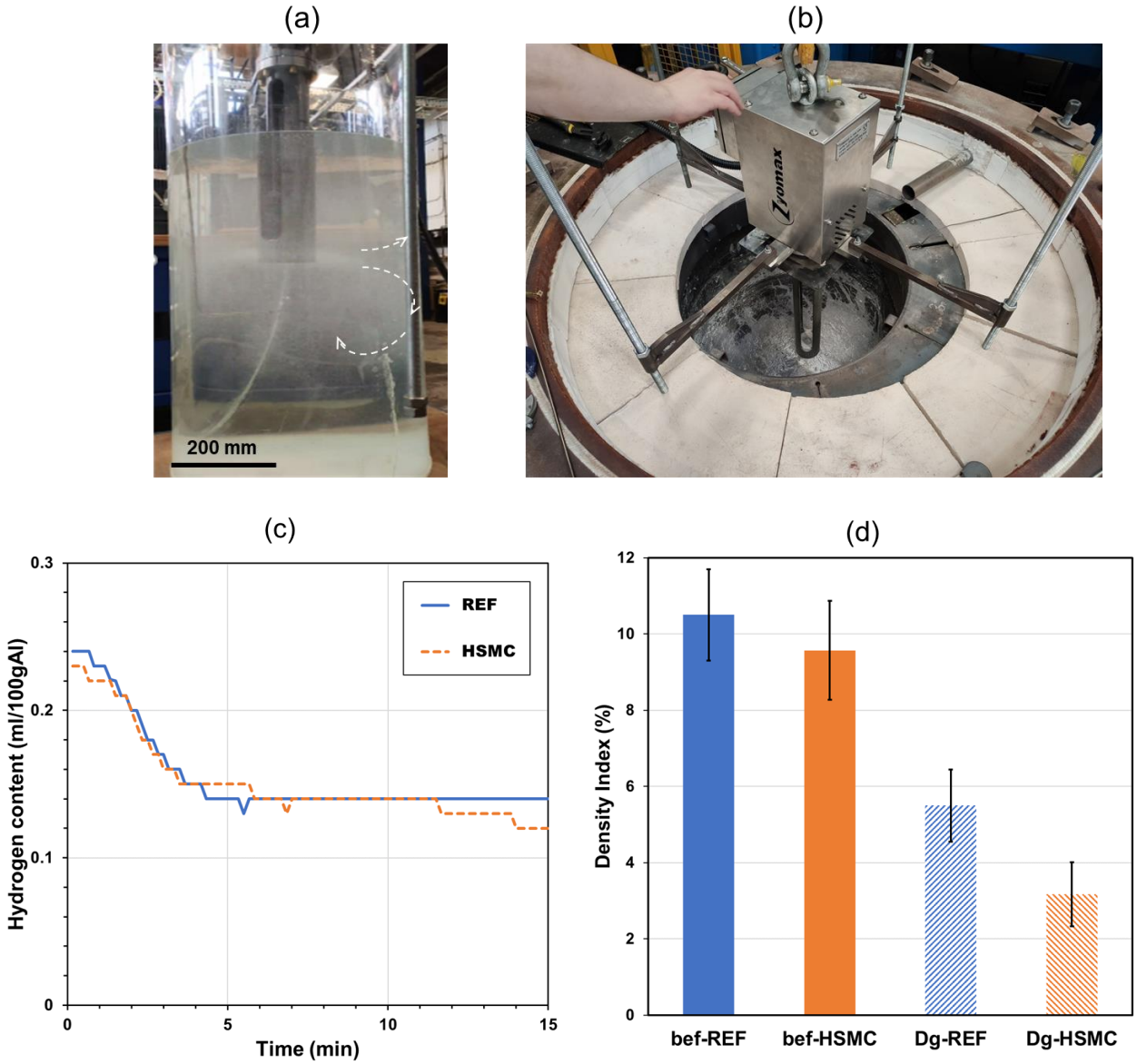

Figure 12. Large-scale activities carried out with the 90 mm HSMC unit for degassing 500 kg A356 aluminum alloy melt. (**a**) Process visualization in water; (**b**) unit implementation in the melt; (**c**) hydrogen level during degassing; (**d**) Density Index before and after degassing.

Firstly, we carried out physical modeling by visualization in water (Figure 12a) in a large plastic tank with similar dimensions to the big crucible (~500 mm diameter). It was found that the optimum processing parameters to achieve an efficient bubble recirculation regime were a rotor speed between 1500 rpm and 2000 rpm and an inert gas flow rate between 0.5 and 1 L/min. These results agree with the expected values from the gas–liquid regime analysis mentioned before in this paper.

After water modeling, a prototype degassing unit was assembled (Figure 12b) to be used as a replacement for the current rotary degasser. The unit is mounted on a light four-legged stand, which provides stability when placed on top of the furnace. The legs can be adjusted horizontally, to accommodate the furnace diameter, and vertically, to vary the immersion depth in the melt. The gas is supplied through an external pipe, fixed underneath the stator. This assembly guarantees an effective bubble capture by the pumping action of the rotor while in operation.

While testing the prototype in the molten aluminum, the hydrogen level was monitored, and the results are compared with the reference results obtained in the same

crucible with the rotary degasser (Figure 12c). Both rotary and HSMC degassing exhibit a similar hydrogen removal rate, but while rotary degassing was performed at 500 rpm with under 15 L/min of Ar gas flow, the HSMC degassing process used a rotor speed of 1500 rpm and an Ar gas flow of only 1 L/min.

Finally, Figure 12d shows the results of melt quality assessment before and after degassing. The melt exhibits a lower Density Index after HSMC degassing, which, considering the similar hydrogen content in the melt, highlights the effective elimination of the undesired oxide bifilms in the melt by means of HSMC. Moreover, rotary degassing was assisted by the flux added into the vortex to help with removing the oxides, while HSMC did not use any flux for the same purpose yet still provided better results.

6.2. HSMC Degassing in Continuous In-Line Processing Mode

Figure 13 shows the schematic diagram of the in-line prototype system designed for continuous melt processing with the HSMC unit [28]. It was prepared by modifying a graphite crucible, such as the one used in the batch processing trials. The melt is poured from one side of the chamber, which incorporates a baffle to direct it toward the bottom of the crucible, where it can be easily captured by the pumping effect of the HSMC unit. On the opposite side, a spout was accommodated on the wall of the chamber to redirect the processed melt out of the system. The capacity of the chamber after these arrangements was about 6 kg. Similar configurations have been developed in recent years, aiming to provide in-line treatment for ultrasound degassing [59].

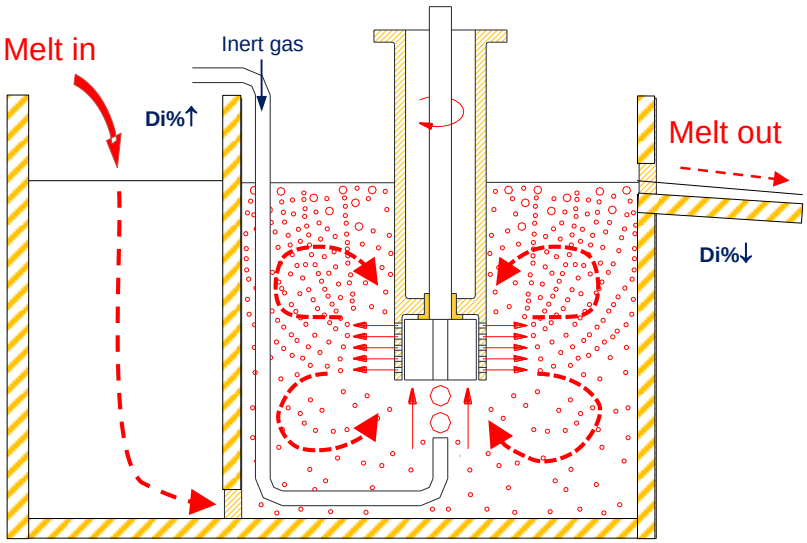

Figure 13. Schematic diagram of the HSMC degassing technology configuration when implemented for continuous in-line processing of aluminum melts. The arrows indicate the flow pattern of the melt and the bubbles in the chamber. Reprinted with permission from [28]. Copyright 2022 Elsevier.

Figure 14 shows the Density Index values as a function of rotor speed, up to 2000 rpm, when the in-line system was tested for degassing the A380 alloy at a melt flow rate of 2 kg/min and at an Argon gas flow rate of 0.1 L/min. The melt quality can be controlled by adjusting the rotor speed. It is, obviously, not fully effective at low speeds, in agreement with what is shown in Figure 3, because the system is not yet in a dispersion or recirculation regime, but the decrease in the Density Index is progressive as the speed increases, falling below 5% for 2000 rpm and expected to be below 3% for 3000 rpm or above, as shown by the included trend line. The results are slightly higher than the ones obtained during batch processing (Figure 5), most likely due to the expected degraded performance, in terms of the mass flow rate through the stator holes, when processing in-

line [38,39], and the limited melt processing time, which is determined by the passage chamber volume and the melt flow rate. In the case shown here, the residence time of the melt in the chamber was approximately 3 min, which, according to Figure 5, is not enough to fully degas the melt by using only 0.1 L/min argon flow and a rotor speed below 3000 rpm.

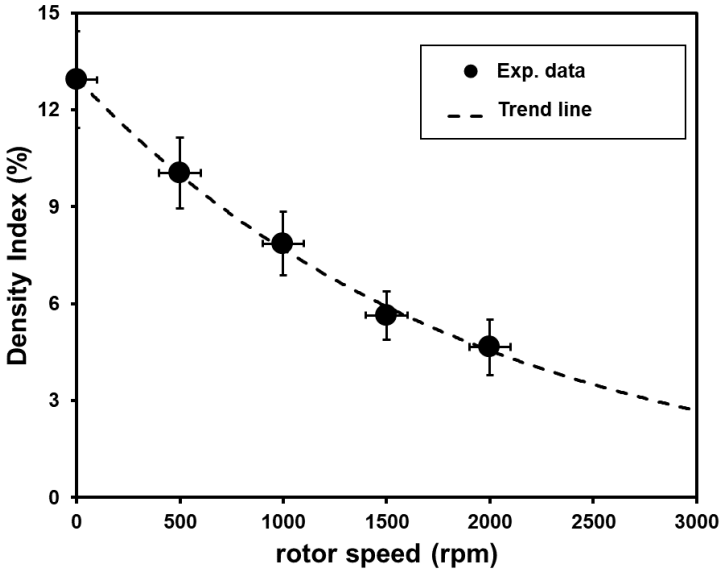

Figure 14. Density Index versus rotor speed during continuous in-line HSMC degassing of an aluminum A380 alloy melt at 700 °C, poured at a melt flow rate of 120 kg/h. Reprinted with permission from [28]. Copyright 2022 Elsevier.

However, a more in-depth analysis of these preliminary results highlights the potential of implementing the technology in continuous mode for melt-quality improvement. Figure 15 shows the internal porosity of the RPT samples solidified under vacuum after in-line HSMC degassing, and Table 2 presents the quantitative analysis on such porosities, in terms of pore size, pore number density, and Bifilm Index (BI). As the rotor speed increases, the size and number density of the pores in the RPT samples decreases, and with those decreases, obviously, the Bifilm Index becomes smaller. According to the interpretations of this parameter [60,61], when the Bifilm Index is lower than 50 mm, the melt can be considered of enough 'good' quality such that the oxide films present have a reduced or minimal effect on the integrity and mechanical failure of the castings. For the samples shown in Figure 15, this threshold value, which ensures good melt quality, is achieved for the rotor speeds between 1500 and 2000 rpm.

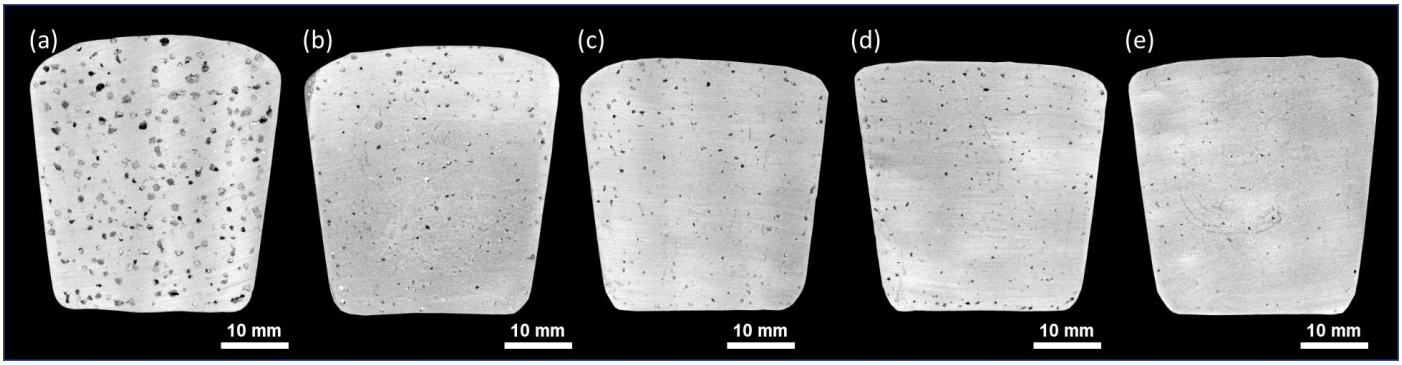

Figure 15. Internal porosity in the RPT samples solidified under partial vacuum during the in-line HSMC degassing process. (**a**) No HSMC; (**b**) 500 rpm; (**c**) 1000 rpm; (**d**) 1500 rpm; (**e**) 2000 rpm. Reprinted with permission from [28]. Copyright 2022 Elsevier.

The continuous mode when implementing HSMC degassing, will obviously, require further modeling and experiments to fully optimize the process' operating conditions and better understand the effect of each parameter, such as chamber size, melt flow, gas flow, alloy type, etc., on the melt quality, but these preliminary results look promising for the easy scalability of this technology toward its final implementation in industrial environments.

7. Summary

- The principle of High Shear Melt Conditioning for the purpose of degassing aluminum melts prior to casting has been technologically developed during the LiME Hub project, providing an efficient solution to solve the aluminum melt cleanliness problem.
- This novel technology guarantees the removal of hydrogen and oxide bifilms at the same time, with a minimal vortex or surface turbulence, something that eliminates the need for protective covering fluxes and minimizes regassing when processing long afterward.
- The optimal parameters for effective bubble recirculation in liquid have been obtained by physical modeling in water. The effective bubble dispersion provided by the HSMC technology allows for drastically reducing the gas flow rate required, in comparison to conventional rotary degassing units and the needs of extremely high rotor speeds, which also reduces the power consumption and makes the process more efficient.
- When HSMC is applied to aluminum melts, a faster and more effective degassing is achieved compared to rotary degassing, because of the dispersive and distributive flow provided by the HSMC technology. The improved melt quality can be guaranteed for a long time after degassing, eliminating the need for repeated degassing cycles and ensuring that the castings have a consistent reduced porosity and enhanced mechanical properties with reduced variability, which allows the aluminum alloys to be upgraded for high-performance applications.
- The melt quality can easily be assessed by a RPT and Density Index calculation, as this an excellent parameter to model and estimate the number of defects present in the castings after degassing and their effect on the decrease in the mechanical properties.
- The HSMC degassing process can be easily implemented in industry, replacing the current conventional rotary impeller technique, with minimal impact on the casting process but with all the benefits of improved melt quality at a reduced cost.
- The current research is focused on scaling up the technology to be used in larger industrial castings, either in batch or in-line configurations and for larger melt quantities or melt flow rates. The implementation in batch with larger units, such as for a 90 mm diameter, requires further optimization, but the preliminary results obtained in large-scale trials have quite promising results and open the possibility for future collaborations with industrial partners to develop an even more efficient degassing process.
- The implementation of the technology for continuous in-line processing has also shown promising possibilities. In-line configuration does not strictly require an increase in the unit size, because the melt flow processing rate can be controlled directly by the chamber size and the rotor speed. In addition, the refinement of the oxide bifilms in the melt can be also controlled by the rotor speed, with high efficiency.

Author Contributions: Conceptualization, J.L-N. and J.B.P.; methodology, investigation, and data analysis and validation, J.L.-N., K.A.-H., E.L., Y.Z., and E.K.; writing—original draft preparation, J.L.-N.; writing—review and editing, J.L.-N., J.B.P.; supervision, project administration, and funding acquisition, J.B.P., G.M.S., and Z.F. All authors have read and agreed to the published version of the manuscript.

Funding: This research was financially supported by the EPSRC (UK) under grant number EP/N007638/1 (the Future Liquid Metal Engineering Hub and LiME Hub).

Institutional Review Board Statement: Not applicable.

Informed Consent Statement: Not applicable.

Data Availability Statement: The data presented in this manuscript are available on request from the corresponding author.

Acknowledgments: The authors would like to thank the support from the Brunel Centre for Advanced Solidification Technology (BCAST), at Brunel University London, where this work was accomplished. The financial support from the EPSRC (UK) under grant number EP/N007638/1 is gratefully acknowledged. The work initiated by Yubo Zuo on this topic is also gratefully appreciated.

Conflicts of Interest: The authors declare no conflicts of interest.

References

1. Zhang, L.; Lv, X.; Torgerson, A.T.; Long, M. Removal of Impurity Elements from Molten Aluminum: A Review. *Miner. Process. Extr. Metall. Rev.* **2011**, *32*, 150–228. https://doi.org/10.1080/08827508.2010.483396.
2. Iwamoto, K.; Yamasaki, M.; Kawamura, Y. Vacuum degassing behavior of rapidly solidified Al-Mn-Zr alloy powders. *Mater. Sci. Eng. A* **2007**, *449–451*, 1013–1017. https://doi.org/10.1016/j.msea.2006.02.252.
3. Eskin, D.; Alba-Baena, N.; Pabel, T.; da Silva, M. Ultrasonic degassing of aluminium alloys: Basic studies and practical implementation. *Mater. Sci. Technol.* **2015**, *31*, 79–84. https://doi.org/10.1179/1743284714Y.0000000587.
4. Wu, R.; Qu, Z.; Sun, B.; Shu, D. Effects of spray degassing parameters on hydrogen content and properties of commercial purity aluminum. *Mater. Sci. Eng. A* **2007**, *456*, 386–390. https://doi.org/10.1016/j.msea.2006.11.094.
5. Warke, V.S.; Shankar, S.; Makhlouf, M.M. Mathematical modelling and computer simulation of molten metal cleansing by the rotating impeller degasser: Part I. Fluid flow. *J. Mater. Process. Technol.* **2005**, *168*, 112–118. https://doi.org/10.1016/j.jmatprotec.2004.10.017.
6. Warke, V.S.; Shankar, S.; Makhlouf, M.M. Mathematical modelling and computer simulation of molten aluminum cleansing by the rotating impeller degasser: Part II. Removal of hydrogen gas and solid particles. *J. Mater. Process. Technol.* **2005**, *168*, 119–126. https://doi.org/10.1016/j.jmatprotec.2004.10.016.
7. Mostafaei, M.; Ghobadi, M.; Ghasem-Eisaabadi, B.; Uludag, M.; Tiryakioglu, M. Evaluation of the Effects of Rotary Degassing Process Variables on the Quality of A357 Aluminum Alloy Castings. *Metall. Mater. Trans. B* **2016**, *47*, 3469–3475. https://doi.org/10.1007/s11663-016-0786-7.
8. Gyarmati, G.; Fegyverneki, G.; Tokár, M.; Mende, T. The Effects of Rotary Degassing Treatments on the Melt Quality of an Al–Si Casting Alloy. *Int. J. Met.* **2021**, *15*, 141–151. https://doi.org/10.1007/s40962-020-00428-z.
9. Fan, Z.; Zuo, Y.B.; Jiang, B. A New Technology for Treating Liquid Metals with Intensive Melt Shearing. *Mater. Sci. Forum* **2011**, *690*, 141–144. https://doi.org/10.4028/www.scientific.net/msf.690.141.
10. Campbell, J. *'Castings'*, 2nd ed.; Butterworth-Heinemann: Oxford, UK, 2003.
11. Tiryakioglu, M. The effect of hydrogen on pore formation in aluminum alloy castings: Myth versus reality. *Metals* **2020**, *10*, 368–385. https://doi.org/10.3390/met10030368.
12. Dispinar, D.; Campbell, J. Critical assessment of reduced pressure test. Part 1: Porosity phenomena. *Int. J. Cast Met. Res.* **2004**, *17*, 280–286. https://doi.org/10.1179/136404604225020696.
13. Dispinar, D.; Campbell, J. Critical assessment of reduced pressure test. Part 2: Porosity phenomena. *Int. J. Cast Met. Res.* **2004**, *17*, 287–294. https://doi.org/10.1179/136404604225020704.
14. Campbell, J. Entrainment defects. *Mater. Sci. Technol.* **2006**, *22*, 127–145. https://doi.org/10.1179/174328406X74248.
15. Ozdes, H.; Tiryakioglu, M. On the relationship between structural quality index and Fatigue Life distributions in aluminum aerospace castings. *Metals* **2016**, *6*, 81. https://doi.org/10.3390/met6040081.
16. Campbell, J.; Tiryakioglu, M. Fatigue failure in engineered components and how it can be eliminated: Case studies on the influence of bifilms. *Metals* **2022**, *12*, 1320. https://doi.org/10.3390/met12081320.
17. Wannasin, J.; Schwam, D.; Wallace, J.F. Evaluation of methods for metal cleanliness assessment in die casting. *J. Mater. Process. Technol.* **2007**, *191*, 242–246. https://doi.org/10.1016/j.jmatprotec.2007.03.013.
18. FOSECO: 'User manual, ALSPEK H', Revision 1.2, Borken, FOSECO 2006. Available online: https://www.environmental-expert.com/files/78789/download/646698/1-ALSPEK_H_GB.pdf (accessed on 27 July 2022).
19. Dispinar, D.; Campbell, J. Use of bifilm index as an assessment of liquid metal quality. *Int. J. Cast Met. Res.* **2006**, *19*, 5–17. https://doi.org/10.1179/136404606225023300.
20. Erzi, E.; Gursoy, O.; Yuksel, C.; Colak, M.; Dispinar, D. Determination of Acceptable Quality Limit for Casting of A356 Aluminium Alloy: Supplier´s Quality Index (SQI). *Metals* **2019**, *9*, 957–971. https://doi.org/10.3390/met9090957.

21. Hernández-Hernández, M.; Cruz-Mendez, W.; González-Rivera, C.; Ramírez-Argáez, M.A. Effect of Process Variables on Kinetics and Gas Consumption in Rotor-Degassing Assisted by Physical and Mathematical Modeling. *Mater. Manuf. Process.* **2015**, *30*, 216–221. https://doi.org/10.1080/10426914.2014.952303.
22. Zuo, Y.B.; Lin, Y.; Kang, Y.Y.; Cui, J.Z. Effects of Rotor Rotation Speed and Gas Flow Rate on the Degassing Efficiency of 2524 Aluminum Alloy in Rotary Degassing Process. *J. Northeast. Univ. Nat. Sci.* **2016**, *37*, 653–657. https://doi.org/10.3969/j.issn.1005-3026.2016.05.010.
23. Uludag, M.; Cetin, R.; Dispinar, D.; Tiryakioglu, M. Characterization of the effect of melt treatments on melt quality in Al-7wt % Si-Mg alloys. *Metals* **2017**, *7*, 157. https://doi.org/10.3390/met7050157.
24. Lazaro-Nebreda, J.; Patel, J.B.; Fan, Z. Improved degassing efficiency and mechanical properties of A356 aluminium alloy castings by high shear melt conditioning (HSMC) technology. *J. Mater. Process. Technol.* **2021**, *294*, 117146. https://doi.org/10.1016/j.jmatprotec.2021.117146.
25. Fan, Z.; Wang, Y.; Xia, M.; Arumuganathar, S. Enhanced heterogeneous nucleation in AZ91D alloy by intensive melt shearing. *Acta Mater.* **2009**, *57*, 4891-4901. https://doi.org/10.1016/j.actamat.2009.06.052.
26. Zuo, Y.; Jiang, B.; Enright, P.; Scamans, G.M.; Fan, F. Degassing of LM24 Al alloy by intensive melt shearing. *Int. J. Cast Met. Res.* **2011**, *24*, 307–313. https://doi.org/10.1179/1743133611Y.0000000002.
27. Camacho-Martínez, J.L.; Ramírez-Argáez, M.; Juárez-Hernández, A.; González-Rivera, C.; Trápaga-Martínez, G. Novel Degasification Design for Aluminum Using an Impeller Degasification Water Physical Model. *Mater. Manuf. Process.* **2012**, *27*, 556–560. https://doi.org/10.1080/10426914.2011.593234.
28. Scamans, G.M.; Li, H.T.; Lazaro-Nebreda, J.; Patel, J.B.; Stone, I.; Wang, Y.; Yang, X.; Fan, Z. Chapter 8-Advanced Casting Technologies Using High Shear Melt Conditioning. In *Fundamentals of Aluminium Metallurgy*; Lumley, R.N.; Woodhead Publishing: Sawston, UK, 2018, https://doi.org/10.1016/B978-0-08-102063-0.00008-4.
29. Tzanakis, I.; Lebon, G.S.B.; Eskin, D.G.; Pericleous, K.A. Characterizing the cavitation development and acoustic spectrum in various liquids. *Ultrason. Sonochemistry* **2017**, *34*, 651–662. https://doi.org/10.1016/j.ultsonch.2016.06.034.
30. Yamamoto, T.; Kato, K.; Komarov, S.V.; Ueno, Y.; Hayashi, M.; Ishiwata, Y. Investigation of melt stirring in aluminum melting furnace through Water model. *J. Mater. Process. Technol.* **2018**, *259*, 409–415. https://doi.org/10.1016/j.jmatprotec.2018.04.025.
31. Kang, Y.Y.; Lin, Y.; Liu, X.D.; Sun, C.; Yuan, S.S.; Zuo, Y.B.; Cui, J.Z. Study on the High Shear Degassing Process with Water Simulation. *Adv. Mater. Res.* **2015**, *1120–1121*, 1214–1219. https://doi.org/10.4028/www.scientific.net/amr.1120-1121.1214.
32. Zuo, Y.B.; Jiang, B.; Zhang, Y.; Fan, Z. Degassing LM25 aluminium alloy by novel degassing technology with intensive melt shearing. *Int. J. Cast Met. Res.* **2013**, *26*, 16–21. https://doi.org/10.1179/1743133612Y.0000000019.
33. Barros, P.L.; Ein-Mozaffari, F.; Lohi, A. Gas dispersion in non-Newtonian fluids with mechanical agitated systems: A Review. *Processes* **2022**, *10*, 275–304. https://doi.org/10.3390/pr10020275.
34. Nienow, A.W. On the Flooding/Loading Transition and the Complete Dispersal Condition in Aerated Vessels Agitated by a Rushton Turbine. In *Proceedings of the of the 5th European Conf. on Mixing, BHRA Cranfield, Wurzburg, Germany, 1985*; BHRA Fluid Engineering: Cranfield, UK, 1985; pp. 143–153.
35. Tatterson, G.B. *Fluid Mixing and Gas Dispersion in Agitated Tanks*; McGraw Hill: New York, USA, 1991.
36. Anza, I.; Mahklouf, M.M. Synthesis of Al-TiC Nanocomposites by an In-Situ Gas-Liquid Method. In *Light Metals*; Williams, E., Ed.; Springer: Cham, Switzerland, 2016. pp. 245-254. https://doi.org/10.1007/978-3-319-48251-4_41.
37. Jamshed, A.; Cooke, M.; Ren, Z.; Rodgers, T. Gas-Liquid Mixing in Dual Agitated Vessels in the Heterogeneous Regime. Chemical Engineering *Res. Des.* **2018**, *133*, 55–69. https://doi.org/10.1016/j.cherd.2018.02.034.
38. Hakansson, A. Rotor-Stator mixers: From batch to continuous mode of operation-A review. *Processes* **2018**, *6*, 32–49. https://doi.org/10.3390/pr6040032.
39. Lebon, G.S.B.; Lazaro-Nebreda, J.; Patel, J.B.; Fan, Z. Numerical Assessment of In-Line Rotor–Stator Mixers in High-Shear Melt Conditioning (HSMC) Technology. *JOM* **2020**, *72*, 4092–4100. https://doi.org/10.1007/s11837-020-04320-3.
40. Zuo, Y.B.; Kang, Y.Y.; Lin, Y.; Zhu, Q.F.; Li, L.; Li, Z.Z.; Cui, J.Z. Dispersion behavior of Ar bubbles under intensive shearing and its effect on degassing effect of 7075 alloy. *Chin. J. Nonferrous Met.* **2016**, *26*, 486–493.
41. Paglianti, A. Simple Model to Evaluate Loading/Flooding Transition in Aerated Vessels Stirred by Rushton Disc Turbines. *Can. J. Chem. Eng.* **2002**, *80*, 1–5. https://doi.org/10.1002/cjce.5450800409.
42. Zhang, Y.; Patel, J.B.; Lazaro-Nebreda, J.; Fan, Z. Improved Defect Control and Mechanical Property Variation in High-Pressure Die Casting of A380 Alloy by High Shear Melt Conditioning. *JOM* **2018**, *70*, 2726–2730, https://doi.org/10.1007/s11837-018-3005-y.
43. Lordan, E.; Lazaro-Nebreda, J.; Zhang, Y.; Fan, Z. Effective Degassing for Reduced Variability in High-Pressure Die Casting Performance. *JOM* **2019**, *71*, 824–830. https://doi.org/10.1007/s11837-018-3186-4.
44. Al-Helal, K.; Lazaro-Nebreda, J.; Patel, J.B.; Scamans, G.M. High-Shear De-Gassing and De-Ironing of an Aluminum Casting Alloy Made Directly from Aluminum End-of Life Vehicle Scrap. *Recycling* **2021**, *6*, 66–76. https://doi.org/10.3390/recycling6040066.
45. Zuo, Y.B.; Kang, Y.Y.; Lin, Y.; Liu, X.; Sun, C.; Yuan, S.; Cui, J. A new high shear degassing technology and mechanism for 7032 alloy. *China Foundry* **2015**, *12*, 293–298.
46. Liu, X.; Zhu, Q.; Zuo, Y.B.; Zhu, C.; Zhao, Z.; Cui, J. Effect of Intensity of melt shearing on the as cast structure of direct chill cast 2024 aluminum alloy. *Metall. Mater. Trans. A* **2019**, *50*, 5727–5733. https://doi.org/10.1007/s11661-019-05452-1.
47. A20X Casting Alloy, Aeromet International Ltd. Available online: https://www.aeromet.co.uk/a20x (accessed on 27 July 2022).

48. *ASTM B108/B108M-19*; Standard Specification for Aluminum-Alloy Permanent Mold Castings. Annual Book of ASTM Standards, vol 02.02. ASTM International: West Conshohocken, PA, USA, 2019. Available online: http://www.astm.org/cgi-bin/resolver.cgi?B108B108M (accessed on 27 July 2022).
49. *ASTM E8-03*; Standard Test Methods for Tension Testing of Metallic Materials. ASTM International: West Conshohocken, PA, USA, 2003. Available online: http://www.astm.org/cgi-bin/resolver.cgi?E8 (accessed on 27 July 2022).
50. Davis, J.R. *Asm Specialty Handbook: Aluminum and Aluminum Alloys*; ASM International: Materials Park, OH, USA, 1993.
51. Galarraga, H.; Cortazar, M.G.; Arregi, E.; Artola, A.; Oncala, J.L.; Merchan, M. Gas blowing ultrasonic Aluminium degassing assessment with the reduced pressure test (RPT) method. *Arch. Foundry Eng.* **2020**, *20*, 111–117, https://doi.org/10.24425/afe.2020.131312.
52. Uludag, M.; Cetin, R.; Gemi, L.; Dispinar, D. Change in porosity of A356 by holding time and its effect on the mechanical properties. *J. Mater. Eng. Perform.* **2018**, *27*, 5141–5151. https://doi.org/10.1007/s11665-018-3534-0.
53. Rosa, D.M.; Spinelli, J.E.; Osorio, W.R.; Garcia, A. Effects of cell size and macrosegregation on the corrosion behavior of a dilute Pb-Sb alloy. *J. Power Sources* **2006**, *162*, 696–705. https://doi.org/10.1016/j.jpowsour.2006.07.016.
54. Donelan, P. Modelling microstructural and mechanical properties of ferritic ductile cast iron. *Mater. Sci. Technol.* **2000**, *16*, 261–269. https://doi.org/10.1179/026708300101507811.
55. Petch, N.J. The cleavage strength of polycrystals. Journal of the Iron and Steel Institute **1953**, *174*, 25–31.
56. Cáceres, C.H.; Selling, B.I. Casting defects and the tensile properties of an Al-Si-Mg alloy. *Mater. Sci. Eng. A* **1996**, *220*, 109–116. https://doi.org/10.1016/S0921-509310433-0.
57. Gyarmati, G.; Fegyverneki, G.; Tokár, M. The effect of inclusions on the tensile properties of AlSi7Mg0.4Cu0.5 casting alloy. *Mater. Sci. Eng.* **2018**, *43*, 54–61.
58. Lordan, E.; Lazaro-Nebreda, J.; Zhang, Y.; Duo, K.; Blake, P.; Fan, Z. On the relationship between internal porosity and the tensile ductility of aluminium alloy die-castings. *Mater. Sci. Eng. A* **2020**, *778*, 139107. https://doi.org/10.1016/j.msea.2020.139107.
59. Eskin, D.G.; Al-Helal, K.; Tzanakis, I. Application of a plate sonotrode to ultrasonic degassing of aluminum melt: Acoustic measurements and feasibility study. *J. Mater. Process. Technol.* **2015**, *222*, 148–154, https://doi.org/10.1016/j.jmatprotec.2015.03.006.
60. Dispinar, D.; Akhtar, S.; Nordmark, A.; Di Sabatino, M.; Arnberg, L. Degassing, hydrogen and porosity phenomena in A356. *Mater. Sci. Eng. A* **2010**, *527*, 3719–3725. https://doi.org/10.1016/j.msea.2010.01.088.
61. Uludag, M.; Cetin, R.; Dispinar, D.; Tiryakioglu, M., 2018. On the Interpretation of Melt Quality Assessment of A356 Aluminum Alloy by the Reduced Pressure Test: The Bifilm Index and Its Physical Meaning. *Int. J. Met.* **2018**, *12*, 853–860. https://doi.org/10.1007/s40962-018-0217-4.